Secondary Ion Mass Spectrometry as a Tool for Investigating Radiopharmaceutical Distribution at the Cellular Level: The Example of I-BZA and ^{14}C-I-BZA

Féras Chéhadé, MD, PhD[1]; Claire de Labriolle-Vaylet, MD, PhD[2]; Nicole Moins, MD, PhD[3]; Marie-France Moreau, PhD[3]; Janine Papon, PhD[3]; Pierre Labarre, PhD[3]; Pierre Galle, MD, PhD[4]; Annie Veyre, MD, PhD[3]; and Elif Hindié, MD, PhD[5]

[1]Nuclear Medicine, Hammoud Hospital University Medical Center, Sidon, Lebanon; [2]Nuclear Medicine, Hopital d'enfants Armand Trousseau, Assistance Publique-Hôpitaux de Paris et Université Paris VI, Paris, France; [3]UMR 484 INSERM-Université d'Auvergne-Centre Jean Perrin, Clermont Ferrand, France; [4]Enrico Fermi Institute, Chicago, Illinois; and [5]Nuclear Medicine, Hôpital Saint Antoine, Assistance Publique-Hôpitaux de Paris, Paris, France

Further development of nuclear medicine for imaging and internal radiotherapy demands a precise knowledge of the tissue and cellular distribution of radiopharmaceuticals. Ion microscopy (secondary ion mass spectrometry [SIMS]) may be particularly useful in this respect. We used SIMS to study the biodistribution of the melanoma-targeting molecule *N*-(2-diethylaminoethyl)-4-iodobenzamide (I-BZA), both in its native state and radiolabeled with ^{14}C. **Methods:** C57BL6/J1/co mice bearing pulmonary colonies of B16 melanoma cells were injected with I-BZA or ^{14}C-I-BZA. Appropriate tissues were fixed and included in epoxy embedding resin for SIMS studies. The distribution of unlabeled I-BZA was studied by detecting its stable iodine atom (^{127}I). ^{14}C-I-BZA distribution was studied by dual detection of ^{127}I and ^{14}C. The time course of I-BZA concentrations at sites of tissue fixation was studied by measuring the signal ratio of ^{14}C and the naturally occurring isotope ^{13}C. **Results:** SIMS showed that I-BZA concentrated in the cytoplasm of tumoral melanocytes (melanoma cells) and in the cytoplasm of tumor-infiltrating macrophages (melanophages). I-BZA was also detected in the cytoplasm of normal melanocytes in the pigmented structures of skin and eye. Interpretation of I-BZA distribution by using electron micrographs of adjacent sections showed that the intracytoplasmic melanin-rich organelles (melanosomes) were responsible for I-BZA retention. The distributions of ^{127}I and ^{14}C after ^{14}C-I-BZA injection were identical, even when I-BZA was separately labeled with ^{14}C at 2 different positions, indicating the stability of the amide bond of I-BZA. The time course of the ^{14}C/^{13}C ratio in the melanosomes of melanoma cells suggested a retention half-life of about 38 h. **Conclusion:** Contrary to previous suggestions that I-BZA fixes principally to σ-1 membrane receptors, our results strongly indicate that I-BZA associates with intracytoplasmic melanin pigments. Early I-BZA accumulation, in both melanocytes and melanophages, suggests that this compound fixes to preformed melanin rather than being incorporated during de novo melanin synthesis. These quantitative and qualitative data obtained with I-BZA illustrate the excellent potential of SIMS for studying the biologic fate of radiopharmaceuticals.

Key Words: SIMS; iodobenzamide; melanoma; radiopharmaceutical; ^{14}C

J Nucl Med 2005; 46:1701–1706

Further therapeutic and diagnostic developments in nuclear medicine demand a better knowledge of radiopharmaceutical distribution (*1,2*). Classic autoradiography and, more recently, β-imagers can be used to study radiopharmaceutical distribution in a given organ, with a resolution close to 50 μm. However, studies of cellular or subcellular distribution require the use of techniques with even higher resolution, such as microautoradiography (*1,3*) and, more recently, ion microscopy (secondary ion mass spectrometry [SIMS]).

Based on mass spectrometric detection, SIMS can offer images of the tissue or cellular distribution of both stable and radioactive atoms (*4–6*). Molecules containing a native halogen atom (fluorine, iodine, or bromine) can be detected without radiolabeling (*7–9*), whereas other molecules must first be labeled with either a stable isotope such as ^{15}N (*10–12*) or a radioactive isotope such as ^{14}C (*10,13,14*).

We used SIMS to study the cellular distribution of *N*-(2-diethylaminoethyl)-4-iodobenzamide (I-BZA), a compound targeting malignant melanoma. Initial studies on animals showed a high concentration ratio between grafted melanomas and various normal tissues (*15*). These results were confirmed in patients with cutaneous or ocular melanoma in a phase II trial with ^{123}I-BZA (*16,17*). Subsequent studies

Received Feb. 7, 2005; revision accepted Jun. 9, 2005.

For correspondence contact: Elif Hindie, MD, PhD, Service de Médecine Nucléaire, Hôpital Saint Antoine, 184 rue du Faubourg Saint Antoine, 75012 Paris, France.

E-mail: elif.hindie@sat.ap-hop-paris.fr

further supported the potential value of I-BZA (*18–20*) and related compounds (*21–26*) for the pathologic staging of melanoma, together with other tracers such as ^{18}F-FDG (*27*).

The high selectivity of I-BZA raises the possibility of therapeutic use in patients with metastatic melanoma, a disease with limited treatment options (*28,29*). However, a precise knowledge of the sites of accumulation in both tumoral and healthy tissues is a prerequisite for clinical use.

The I-BZA fixation site is controversial. John et al. (*21–22*) and others (*20,30*) have suggested that I-BZA and the related analog 2-piperidinylaminoethyl-4-iodobenzamide accumulate in melanomas by binding to σ-receptors on the cell membranes (*20–22,30*). Competitive binding studies using guinea pig brain membranes and (^{3}H)(+)-pentazocine, a selective σ-1 ligand, showed that both I-BZA and the related analog had high affinity for σ-1 sites. However, Chehade et al. (*31*) and others (*23,24,32*) have suggested that I-BZA fixes preferentially to melanin granules. Proponents of this second hypothesis disagree on the underlying mechanism. Dittmann suggests that I-BZA is incorporated during melanin synthesis (*23*), whereas Labarre suggests that I-BZA binds to preformed melanin (*32*).

The SIMS images presented here were obtained with various tissue samples from mice bearing pulmonary colonies of melanoma B16 cells. The study comprised 3 steps: We first used an IMS-4F scanning ion microscope (CAMECA) to map the distribution of unlabeled I-BZA in tumor tissue and normally pigmented tissues (eye and skin) by detecting the stable ^{127}I atom. Our initial observations (*31,33*), obtained with a first-generation low-resolution ion microscope (SMI-300; CAMECA), allowed us to select the tissue regions of interest for this study. We then compared images of ^{127}I distribution with those of a ^{14}C radiolabel. Separate experiments were performed with I-BZA labeled by ^{14}C at 2 different positions, to obtain further information on the structure of the molecule at its tissue-binding site. Finally, we studied the time course of ^{14}C-I-BZA concentrations at cellular retention sites.

MATERIALS AND METHODS

This study was performed in keeping with French legislation on animal experimentation.

Tumor Model, ^{127}I-BZA Administration, and Tissue Preparation

B16 murine melanoma cells were injected intravenously into adult male C57BL6/J1/co mice (Iffa Credo) to obtain tumor cell colonies mimicking pulmonary micrometastases (*33*). Briefly, transplantable B16 mouse melanoma cells, obtained from Institut de Cancérologie et Immuno-Génétique, were maintained as monolayers in minimal essential medium supplemented with 10% fetal bovine serum and antibiotics and passaged by trypsinization. For transplantation, melanoma cells were trypsinized and washed with phosphate-buffered saline, then resuspended in phosphate-buffered saline (1.5×10^6 viable cells per milliliter); 0.2 mL of this suspension was injected intravenously. Multiple tumor colonies developed in the lungs within 3 wk.

I-BZA was injected into tumor-bearing and control animals via a tail vein (2.6 μmol per animal). Three groups of tumor-bearing and control animals were sacrificed by CO_2 inhalation at different times. The lungs, eyes, and tail skin were removed, fixed with glutaraldehyde, and embedded in epoxy resin. To verify that the fixation steps do not lead to significant release of the compound, we measured radioactivity in the solutions during each step of tissue preparation. This was done in our early animal studies using ^{125}I-BZA (*15*) and confirmed with ^{14}C-I-BZA.

Serial 2-μm-thick slices were placed on gold plates for SIMS and on glass slides for light microscopy. Samples were also prepared for electron microscopy.

SIMS

The basic principles of this method are described in detail elsewhere (*4*). In a SIMS device, the tissue section is bombarded with ions with an energy of about 15 keV, known as the primary ion beam. This bombardment breaks most chemical bonds, and the atoms constituting the sample are ejected ("sputtered"). The sample is gradually sputtered, starting with the most superficial layers of atoms. Atoms are ejected from the sample surface as charged particles and are guided by an electrostatic field, resulting in a secondary ion beam. The latter is directed toward a mass spectrometer tuned to detect a given ion species, yielding an image that reflects the distribution of the selected ion species.

The ejected iodine atoms are detected by SIMS in the form of negatively charged ions ($^{127}I^-$). The resulting map of ^{127}I distribution reflects the tissue and cellular distribution of I-BZA or its metabolites. The distribution of ^{14}C-I-BZA is visualized by dual detection of $^{127}I^-$ and $^{14}C^-$ ions (*10,14*). Tissue structures can also be identified by SIMS, by detecting highly emissive CN^- polyatomic ions, which reflect tissue and intracellular nitrogen content, or by imaging the distribution of sulfur ions ($^{32}S^-$). Imaging of phosphorus ions ($^{31}P^-$), which are mainly emitted from nucleic acids, can be used to identify the cell nucleus.

The instrument used for this study was an IMS-4F scanning ion microscope. Samples were bombarded with a primary beam of positively charged cesium ions (Cs^+), offering high yields of $^{127}I^-$ and $^{14}C^-$. The minimum diameter of the Cs^+ beam in this device is 0.3 μm, offering a resolution of 0.5–1 μm on the recorded images. Analyses were performed at a high mass resolution ($M/\Delta M = 3{,}000$) to avoid interference by polyatomic groups. Indeed, a mass resolution of $M/\Delta M \geq 1{,}750$ is necessary to separate $^{14}C^-$ (14.0032 amu) from the closest interference due to $^{13}C^1H^-$ (14.0112 amu) (*10,14*). The selected ions are counted by the detector (an electron multiplier), directly yielding digital distribution images.

^{14}C Labeling and Comparison of ^{127}I and ^{14}C Distribution

To assess the stability of the amide bond (CO-NH), we separately labeled I-BZA with ^{14}C at 2 positions on either side of this bond—precisely, on the carbonyl group I-ϕ-^{14}CO-NH-CH_2-CH_2-$N[C_2H_5]_2$ (^{14}C-BZA-carbonyl, 151.7 kBq/μmol) and the *N*-diethylamine group I-ϕ-CO-NH-CH_2-$^{14}CH_2$-$N[C_2H_5]_2$ (^{14}C-BZA-amine, 188.7 kBq/μmol). The status of the carbon chain (intact/broken) was determined by comparing the images of ^{127}I and ^{14}C distribution.

Estimation of Retention Half-Life of I-BZA at Cellular Level

^{14}C labeling was also used to study the time course of I-BZA concentrations at the sites of retention.

The iodine signal cannot be used to compare I-BZA concentrations from one field to another or from one sample to another, because it is susceptible to the experimental conditions. In contrast, this comparison is possible for a ^{14}C-labeled compound (*14*), by measuring the local isotopic ratio between ^{14}C and 1 of the 2 stable, naturally occurring carbon isotopes, ^{12}C or ^{13}C. We chose to measure the ^{14}C/^{13}C ratio rather than the ^{14}C/^{12}C ratio because ^{12}C, being highly abundant, can saturate the detector. The isotopic abundance of ^{13}C is close to 1.1%. Naturally occurring ^{14}C, which has an isotopic abundance of 1.2×10^{-12}, yields no signal under our analytic conditions (data not shown).

RESULTS

SIMS images were obtained with tissues sampled 3 h after I-BZA injection. (According to Michelot et al., uptake is maximal as early as the first hour (*15*).)

I-BZA Distribution in Epidermal Layer of Skin

Figure 1 shows SIMS images of mouse tail skin (field, 50×50 μm). Part A shows the distribution of CN^- ions (mass, 26), revealing various tissue structures, including, from top to bottom, the stratum corneum, the other epidermal layers, and the superficial dermis. Part B shows the distribution of phosphorus (mass, 31), clearly identifying the cell nuclei, especially in the deeper epidermis. The most emissive structures correspond to nuclear membranes (heterochromatin) and nucleoli. Part C shows the distribution of iodine (mass, 127). Several distinct foci of uptake are visible, each with a size approaching 1 μm. These foci are especially abundant in the deeper epidermis. Part D shows superimposed artificially colored images, in which green corresponds to phosphorus and red to iodine. The red foci in the basal epidermis show an intracytoplasmic, perinuclear distribution.

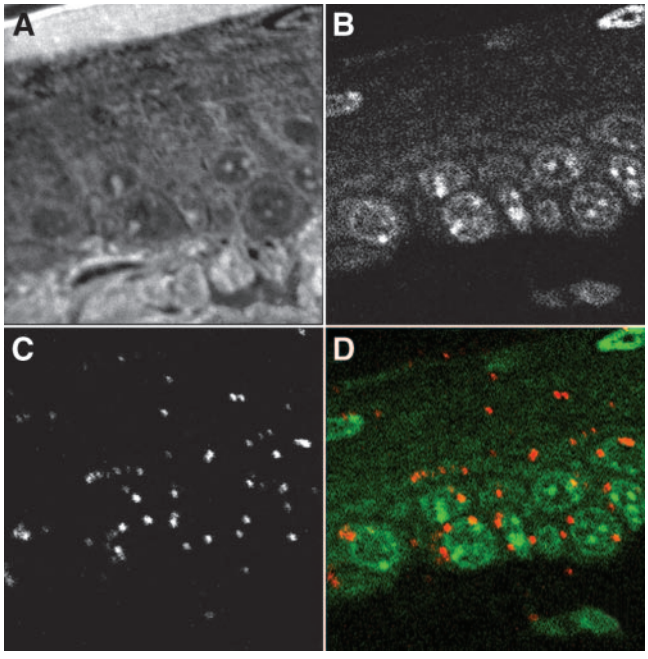

FIGURE 1. SIMS images of a 50×50 μm field of skin: distribution of $^{26}CN^-$ ions (A), $^{31}P^-$ ions (B), and $^{127}I^-$ ions (C) and superimposition of iodine signal in red and of phosphorus signal in green (D).

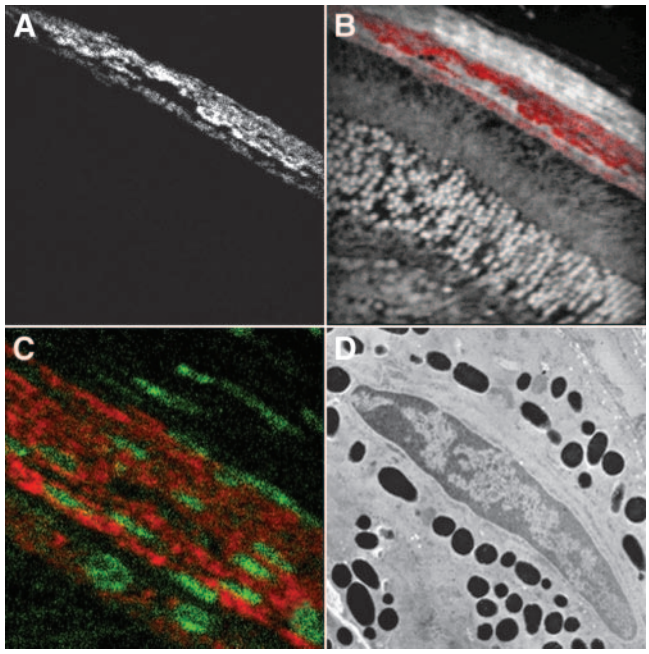

FIGURE 2. (A and B) SIMS images of a 200×200 μm field of eye: distribution of ^{127}I (A) and superimposition of iodine signal in red and of CN signal in gray (B). (C) Superimposition of iodine signal in red and of phosphorus signal in green in a 50×50 μm field centered on choroid and pigmentary epithelium. (D) Electron micrograph of choroidal melanocytes in a 6×6 μm field.

I-BZA Distribution in Choroid and Pigmented Retinal Epithelium

Figures 2A and 2B are SIMS images of an ocular section (field, 200×200 μm). Part A shows the tissue distribution of ^{127}I, with 2 parallel bands. Part B, a superimposition of the ^{127}I signal (red) on the ^{26}CN signal (gray), shows that the broadest (outer) band corresponds to the choroid and the thinnest band to the pigmented retinal epithelium. The other ocular layers seen on the ^{26}CN map (the outer sclerotic and the inner layers corresponding to the cones and rods and to the nuclei of these cells) show no I-BZA uptake.

We then focused on a 50×50 μm field that included the choroid and pigmented retinal epithelium. Figure 2C shows superimposed ^{31}P (green) and ^{127}I (red) signals. The ^{31}P signal shows 2 nuclear aspects: The elongated nuclei correspond to the choroid, and the more rounded nuclei to the underlying pigmented epithelium. As in the skin, the ^{127}I uptake foci are located in the cytoplasm.

Figure 2D is an electron micrograph of the principal cell—melanocytes—constituting the choroid. Comparison of this image with the ion micrograph suggests that the multiple bright cytoplasmic foci of ^{127}I correspond to melanosomes, the intracytoplasmic organelles that synthesize melanin (*34*). Melanosomes are abundant in the cytoplasm of choroidal melanocytes, explaining why the iodine signal is intense and nearly confluent in these cells.

I-BZA Distribution in Pulmonary Melanoma Cell Colonies

Figures 3A and 3B are SIMS images of a murine B16 melanoma cell colony developing in the alveolar parenchyma (field, 60 × 60 μm). Part A shows that the tissue distribution of ^{127}I is highly heterogeneous. There are multiple small, scattered foci measuring 1 μm or less. There is also a larger, ^{127}I-rich, site about 15 μm in diameter. Part B shows the superimposition of the ^{31}P image (green, representing nuclei) and the ^{127}I image (red): The 2 signals are distinct, confirming that I-BZA has no nuclear location.

Comparison with the electron micrographs (Figs. 3C and 3D) facilitates cell identification and helps explain the iodine distribution. Most of the cells composing the tumor are tumoral melanocytes, and their cytoplasm contains small melanosomes of variable shape (Fig. 3C). The cell containing abundant iodine corresponds to a tumor-infiltrating macrophage (melanophage). These cells show multiple intracytoplasmic complexes, containing melanosomes and other melanin-rich phagocytotic products (Fig. 3D).

Comparison of ^{127}I and ^{14}C Distribution

After Injection of ^{14}C-I-BZA Amine. SIMS images obtained 1, 14, and 72 h after injection showed a similar distribution of ^{14}C and ^{127}I, both in the eye and in pulmonary colonies of B16 melanoma cells. Figure 4 shows SIMS images of the eye 1 h after injection. Part A shows superimposed images of the phosphorus signal (green) and the iodine signal (red). Part B shows superimposed images of the ^{31}P signal (green) and the ^{14}C signal (violet). These images confirm the similar topography of ^{14}C and ^{127}I, both of which are found in the cytoplasm of melanocytes present in the choroid and retinal pigmented epithelium. The ^{127}I images are more strongly contrasted than the ^{14}C images because ^{127}I, a readily ionized halogen, has a stronger SIMS yield than does ^{14}C. The specificity of I-BZA and ^{14}C-I-BZA imaging was assessed by studying controls prepared under the same conditions.

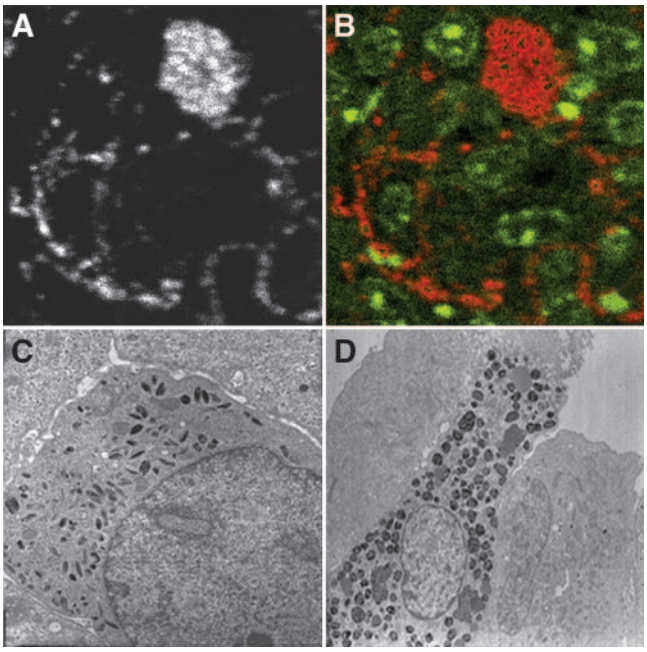

FIGURE 3. (A and B) SIMS images of a 60 × 60 μm field focusing on part of a pulmonary colony of B16 melanoma: distribution of ^{127}I (A) and superimposition of iodine signal in red and of phosphorus signal in green (B). (C) Electron micrograph of a melanoma cell in an 8 × 8 μm field. (D) Electron micrograph of a tumor-infiltrating macrophage (melanophage) in a 23 × 23 μm field.

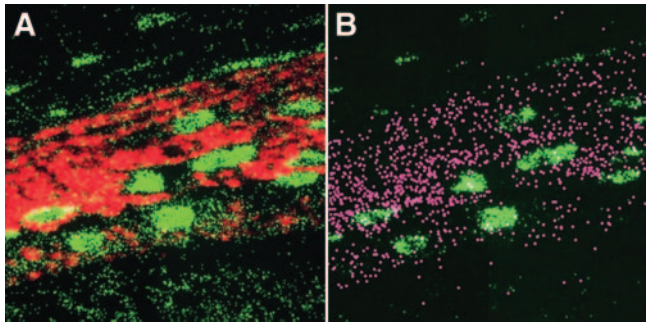

FIGURE 4. SIMS images of a 50 × 50 μm field centered on choroid and retinal pigmented epithelium, 1 h after ^{14}C-I-BZA amine injection: superimposition of iodine signal in red and of phosphorus signal in green (A), and superimposition of ^{14}C signal in violet and of phosphorus signal in green (B).

After Injection of ^{14}C-I-BZA-Carbonyl. Here too, the analysis of images obtained at 2 different times (2 and 14 h after injection) showed that the distributions of ^{127}I and ^{14}C were identical in the pigmented eye layers and in pulmonary colonies of B16 melanoma cells.

Biologic Half-Life of I-BZA in Melanosomes of Melanoma Cells

In view of the imaging results, we studied the time course of the ^{14}C/^{13}C ratio in the cytoplasm of tumoral melanocytes. Intracytoplasmic measurements were focused on regions of interest (1.6 × 1.6 μm) encompassing foci of ^{14}C (melanosomes and intracytoplasmic melanin granules). At each time point (1, 14, and 72 h) after injection of ^{14}C-I-BZA amine, an average of 170 measurements was made.

The ^{14}C/^{13}C ratio gradually fell in tumoral melanosomes, from a mean value of 13×10^{-5} ($\pm 12 \times 10^{-5}$) at the first hour to 10×10^{-5} ($\pm 6 \times 10^{-5}$) at 14 h and then 3.6×10^{-5} ($\pm 2.3 \times 10^{-5}$) at 72 h. On the basis of these data, the estimated retention half-life of ^{14}C-I-BZA in tumoral melanosomes was about 38 h.

DISCUSSION

Site of I-BZA Retention

This study settles the controversy over the I-BZA retention site in melanoma cells—that is, membrane σ-1 receptors (*20–22,30*) or melanin (*23,24,32*). The high I-BZA concentration in the cytoplasm of normal and tumoral melanocytes and its pattern of distribution on SIMS images clearly favor the second hypothesis. Thus, when melanin is

present, the melanin binding is the one apparent. Any specific binding to σ-membrane receptors would contribute little to the total amount of I-BZA retained in melanomas or normal pigmented tissues. We had early raised the hypothesis that I-BZA was specifically located in melanin granules (*31*). In that earlier work, however, we had to combine 2 microanalytic techniques: SIMS analysis with the low-resolution ion microscope SMI-300, and electron probe x-ray microanalysis. The SMI-300 had shown that I-BZA was specifically located in the choroidal melanocytes and retinal pigment cells. Then, when the beam of the electron microscope was focused on various intracellular structures, the characteristic Lα1 x-rays of iodine were specifically detected in the melanin granules of the melanosomes (*31*). The results obtained here with the better-resolution IMS-4F ion microscope on the eye, skin, and melanoma tissues corroborate our previous findings. Further improvement in spatial resolution is now possible with the advent of a new generation of ion microscopes, such as the NanoSIMS-50 (CAMECA) (*35*), as borne out during work on a prototype (*10,11*) and also during preliminary work on the commercialized instrument (*36*).

Melanins are polymers synthesized by melanocytes (*34*). Many compounds accumulate in pigmented tissues, either by incorporation in nascent melanin (*34*) or by binding to preformed melanin (*37*). The significant accumulation of I-BZA observed here, not only in melanoma cells but also in melanoma-infiltrating macrophages (melanophages), as early as 1 h after injection favors binding to preformed melanin. Indeed, melanophages do not synthesize melanin but phagocytose melanin pigment and melanosome bodies released by melanocytes. The presence of I-BZA in the pigmented layers of the retina also supports this view, because this tissue contains mainly mature melanosomes, with little or no melanin turnover after birth (*34*).

Comparison of ^{127}I and ^{14}C Images

SIMS offered far more information than did a simple distribution map. The distribution of ^{127}I and that of the 2 I-BZA species labeled with ^{14}C at different molecular sites were identical, indicating the stability of the amide bond of I-BZA. To our knowledge, this is the first SIMS work assessing the intracellular metabolic state of a molecule by comparing images of atoms present at different sites of the studied molecule.

As with any tracer study, one should consider the possibility of redistribution of the compound during the fixation steps. However, the images obtained of various tissues (normal and tumoral), consistently showing I-BZA uptake by intracytoplasmic melanosomes, strongly suggest a specific uptake mechanism. Moreover, our results agree with those of other authors, who used either cell cultures (*23*) or centrifugation techniques (*24*).

Some authors have applied cryogenic techniques successfully to SIMS using, for example, a cryogenic sandwich-fracture method for cell cultures followed by freeze-drying (*5*).

Quantitative Cellular Data

The ^{14}C/^{13}C ratio can be used to study concentration variations in different cells and to calculate the biologic half-life at retention sites. Our measurements of the ^{14}C/^{13}C ratio in samples taken at different times after ^{14}C-I-BZA injection yielded a calculated biologic half-life of 38 h in tumor-cell melanosomes.

SIMS and Microdosimetry

When presenting MIRD pamphlet no. 17, Bolch et al. underlined the limitations of macroscopic dosimetry, especially in applications such as internal cancer radiotherapy (*1*). Indeed, the therapeutic efficacy of new radiopharmaceuticals can be difficult to predict with this method because of a lack of information on the precise tissue distribution.

The digital images provided by SIMS can be used directly to assess the distribution of the radiopharmaceutical as basic data for dose calculations on the cell and tissue level. We found that I-BZA was present both in tumor-cell melanocytes and in melanophages. The latter are less numerous but contain higher I-BZA concentrations. Monte Carlo techniques can now be used to determine the dose distribution for a given isotope, taking into account the distribution as imaged by SIMS (*2,38,39*).

SIMS circumvents certain limitations of microautoradiography, such as the difficulty of matching the position in the emulsion with the cellular site of radioactive emission, the difficulty of assessing local concentrations (yield quantification is imprecise in microautoradiography), and the poor sensitivity of microautoradiography for ^{14}C (physical half-life, 5,730 y).

Implications of Our Results

Although our results cannot be directly extrapolated to humans, they show that I-BZA may be a useful compound for internal radiotherapy. I-BZA is incorporated by melanoma tumor tissue, within melanocytes and melanophages. Its half-life at its cellular retention site was approximately 38 h in the model used here. Thus, internal radiotherapy seems to be a promising approach for melanoma treatment.

The I-BZA uptake ratio between tumoral and healthy tissues (blood, muscle, brain, lung, and liver) is high (*15,18*). However, because I-BZA is also taken up by the melanocytes of normal pigmented tissues, studies of the possible impact on these tissues will be needed.

CONCLUSION

This study contributes to the debate on the retention site of I-BZA, a compound of potential interest for the imaging and treatment of malignant melanoma. Our results also show that ionic microscopy (SIMS) is a potent tool for the development and assessment of labeled and unlabeled radiopharmaceuticals.

ACKNOWLEDGMENTS

We thank Pr. Georges Slodzian and Royer Dennebouy for having hosted imaging studies on the IMS-4F ion microscope, installed at Laboratoire de Physique des Solides (Paris XI University).

REFERENCES

1. Bolch WE, Bouchet LG, Robertson JS, et al. MIRD Pamphlet No. 17: the dosimetry of nonuniform activity distributions—radionuclide S values at the voxel level. Medical Internal Radiation Dose Committee. *J Nucl Med.* 1999; 40(suppl):11S–36S.
2. Goddu SM, Rao DV, Howell RW. Multicellular dosimetry for micrometastases: dependence of self-dose versus cross-dose to cell nuclei on type and energy of radiation and subcellular distribution of radionuclides. *J Nucl Med.* 1994;35:521–530.
3. Puncher MR, Blower PJ. Radionuclide targeting and dosimetry at the microscopic level: the role of microautoradiography. *Eur J Nucl Med.* 1994;21:1347–1365.
4. Galle P. Tissue localization of stable and radioactive nuclides by secondary ion microscopy. *J Nucl Med.* 1982;23:52–57.
5. Chandra S, Lorey DR. SIMS ion microscopy in cancer research: single isotopic imaging for chemical composition, cytotoxicity and cell cycle recognition. *Cell Mol Biol.* 2001;47:503–518.
6. Hindie E, Petiet A, Bourahla K, et al. Microscopic distribution of iodine radioisotopes in the thyroid of the iodine deficient new-born rat: insight concerning the Chernobyl accident. *Cell Mol Biol.* 2001;47:403–410.
7. Hindie E, Coulomb B, Escaig F, Galle P. Intracellular dynamics of the fluorinated drug, dexamethasone. In: Benninghoven A, ed. *Secondary Ion Mass Spectrometry: SIMS VI.* Chichester, U.K.: John Wiley; 1988:881–884.
8. Clerc J, Halpern S, Fourre C, et al. SIMS microscopy imaging of the intratumor distribution of metaiodobenzylguanidine in the human SK-N-SH neuroblastoma cell line xenografted into nude mice. *J Nucl Med.* 1993;34:1565–1570.
9. Chehade F, Maurizis JC, Pucci B, et al. Subcellular distribution of a new fluorinated, biocompatible, non-ionic telomeric carrier: a study in cultured B16 melanoma and rat skin fibroblasts. *Cell Mol Biol.* 1996;42:335–342.
10. Hindie E, Coulomb B, Beaupain R, Galle P. Mapping the cellular distribution of labelled molecules by SIMS microscopy. *Biol Cell.* 1992;74:81–88.
11. Hindie E, Slodzian G, Beaupain R, et al. High resolution intracellular mapping of nitrogen-15-labelled molecules. In: Benninghoven A, ed. *Secondary Ion Mass Spectrometry: SIMS VIII.* Chichester, U.K.: John Wiley; 1992:677–680.
12. Peteranderl R, Lechene C. Measure of carbon and nitrogen stable isotope ratios in cultured cells. *J Am Soc Mass Spectrom.* 2004;15:478–485.
13. Hindie E, Hallegot P, Chabala JM, et al. Ion microscopy: a new approach for subcellular localization of labelled molecules. *Scanning Microsc.* 1988;2:1821–1829.
14. Hindie E, Coulomb B, Galle P. SIMS microscopy: a tool to measure the intracellular concentration of carbon-14-labelled molecules. *Biol Cell.* 1992;74: 89–92.
15. Michelot JM, Moreau MFC, Labarre P, et al. Synthesis and evaluation of new iodine-125 radiopharmaceuticals as potential tracers for malignant melanoma. *J Nucl Med.* 1991;32:1573–1580.
16. Michelot JM, Moreau MFC, Veyre AJ, et al. Phase II scintigraphic clinical trial of malignant melanoma and metastases with iodine-123-N-(2-diethylaminoethyl)-4-iodobenzamide. *J Nucl Med.* 1993;34:1260–1266.
17. Rodot S, Darcourt J, Bussiere F, et al. A radiolabelled iodobenzamide for malignant melanoma staging. *Melanoma Res.* 1994;4:307–312.
18. Brandau W, Kirchner B, Bartenstein P, Sciuk J, Kamanabrou D, Schober O. N-(2-diethylaminoethyl)-4-(^{123}I) iodobenzamide as a tracer for the detection of malignant melanoma: simple synthesis, improved labelling technique and first clinical results. *Eur J Nucl Med.* 1993;20:238–243.
19. Everaert H, Bossuyt A, Flamen P, Mertens J, Franken PR. Visualizing ocular melanoma using iodine-123-N-(2-diethylaminoethyl)4-iodobenzamide SPECT. *J Nucl Med.* 1997;38:870–873.
20. Everaert H, Flamen P, Franken PR, Verhaeghe W, Bossuyt A. Sigma receptor imaging by means of ^{123}I-IDAB scintigraphy: clinical application in melanoma and non-small cell lung cancer. *Anticancer Res.* 1997;17:1577–1582.
21. John CS, Bowen WD, Saga T, et al. A malignant melanoma imaging agent: synthesis, characterisation, in vitro binding and biodistribution of iodine-125-(2-piperidinylaminoethyl)4-iodobenzamide. *J Nucl Med.* 1993;34:2169–2175.
22. John CS, Baumgold J, Vilner BJ. (^{125}I)N-(2-piperidinylaminorthyl) 4-iodobenzamide and related analogs as sigma receptor imaging agents; high affinity binding to human malignant melanoma and rat C6 glioma cell lines. *J Labelled Compds Radiopharm.* 1994;35:242–244.
23. Dittmann H, Coenen HH, Zölzer F, Dutschka K, Brandau W, Streffer C. In vitro studies on the cellular uptake of melanoma imaging aminoalkyl-iodobenzamide derivatives (ABA). *Nucl Med Biol.* 1999;26:51–56.
24. Eisenhut M, Hull WE, Mohammed A, et al. Radioiodinated N-(2-diethylaminoethyl)benzamide derivatives with high melanoma uptake: structure-affinity relationships, metabolic fate, and intracellular localization. *J Med Chem.* 2000;43: 3913–3922.
25. Moins N, D'Incan M, Bonafous J, et al. ^{123}I-N-(2-diethylaminoethyl)-2-iodobenzamide: a potential imaging agent for cutaneous melanoma staging. *Eur J Nucl Med.* 2002;29:1478–1484.
26. Sillaire-Houtmann I, Bonafous J, Veyre A, et al. Phase 2 clinical study of ^{123}I-N-(2-diethylaminoethyl)-2-iodobenzamide in the diagnostic of primary and metastatic ocular melanoma [in French]. *J Fr Ophtalmol.* 2004;27:34–39.
27. Wong C, Silverman DH, Seltzer M, et al. The impact of 2-deoxy-2(^{18}F)fluoro-D-glucose whole body positron emission tomography for managing patients with melanoma: the referring physician's perspective. *Mol Imaging Biol.* 2002;4:185–190.
28. Eigentler TK, Caroli UM, Radny P, Garbe C. Palliative therapy of disseminated malignant melanoma: a systematic review of 41 randomised clinical trials. *Lancet Oncol.* 2003;4:748–759.
29. Keilholz U, Gore ME. Biochemotherapy for advanced melanoma. *Semin Oncol.* 2002;29:456–461.
30. Caveliers V, Everaert H, Lahoutte T, Dierickx LO, John CS, Bossuyt A. Labelled sigma receptor ligands: can their role in neurology and oncology be extended? *Eur J Nucl Med.* 2001;28:133–135.
31. Chehade F, Michelot J, Hindié E, et al. Localization of N-(2-diethylaminoethyl)-4-iodobenzamide in the pigmented mouse eye: a microanalytical study. *Cell Mol Biol.* 1996;42:343–350.
32. Labarre P, Papon J, Moreau M-F, et al. Melanin affinity of N-(2-diethylaminoethyl)-4-iodobenzamide, an effective melanoma imaging agent. *Melanoma Res.* 2002;12:115–121.
33. Chehade F, de Labriolle-Vaylet C, Michelot J, et al. Distribution of I-BZA (N-2-diethylaminoethyl-4-iodobenzamide) in grafted melanoma and normal skin: a study by secondary ion mass spectroscopy. *Cell Mol Biol.* 2001;47:529–534.
34. Lindquist NG, Larsson BS, Stjernschantz J, Sjöquist B. Age-related melanogenesis in the eye of mice, studied by microautoradiography of ^{3}H-methimazole, a specific marker of melanin synthesis. *Exp Eye Res.* 1998;67:259–264.
35. Slodzian G, Daigne B, Girard F, Boust F, Hillion F. Scanning secondary ion analytical microscopy with parallel detection. *Biol Cell.* 1992;74:43–50.
36. Guerquin-Kern JL, Hillion F, Madelmont JC, Labarre P, Papon J, Croisy A. Ultra-structural cell distribution of the melanoma marker iodobenzamide: improved potentiality of SIMS imaging in life sciences. *Biomed Eng Online.* 2004;3:1–7.
37. Larsson BS. Interaction between chemicals and melanin. *Pigment Cell Res.* 1993;6:127–133.
38. Li WB, Friedland W, Pomplun E, et al. Track structures and dose distributions from decays of (131)I and (125)I in and around water spheres simulating micrometastases of differentiated thyroid cancer. *Radiat Res.* 2001;156:419–429.
39. Champion C. Theoretical cross sections for electron collisions in water: structure of electron tracks. *Phys Med Biol.* 2003;48:2147–2168.

JNM The Journal of NUCLEAR MEDICINE

Secondary Ion Mass Spectrometry as a Tool for Investigating Radiopharmaceutical Distribution at the Cellular Level: The Example of I-BZA and ^{14}C-I-BZA

Féras Chéhadé, Claire de Labriolle-Vaylet, Nicole Moins, Marie-France Moreau, Janine Papon, Pierre Labarre, Pierre Galle, Annie Veyre and Elif Hindié

J Nucl Med. 2005;46:1701-1706.

The Journal of Nuclear Medicine is published monthly.
SNMMI | Society of Nuclear Medicine and Molecular Imaging
1850 Samuel Morse Drive, Reston, VA 20190.
(Print ISSN: 0161-5505, Online ISSN: 2159-662X)

SNMMI SOCIETY OF NUCLEAR MEDICINE AND MOLECULAR IMAGING